Journal of Al-Azhar University Engineering Sector

Vol. 19, No. 70, January 2024, 25 - 50

MECHANICAL PROPERTIES AND MICROSTRUCTURE OF HIGH-STRENGTH ALKALI-ACTIVATED CONCRETE INCLUDING HIGH-VOLUMES OF WASTE BRICK POWDER USING RESPONSE SURFACE METHODOLOGY

Salah K. Alkhurainej*, Mohamed G Mahdy, Ahmed M. Tahwia

Dep. of Structural Eng., Faculty of Engineering, Mansoura University, Egypt

***Correspondence:** E-mail: mng_salah@outlook.com

Citation:

S. K. Alkhurainej, M. G Mahdy, and A. M. Tahwia, "Mechanical Properties And Microstructure Of High-Strength Alkali-Activated Concrete Including High-Volumes Of Waste Brick Powder Using Response Surface Methodology", Journal of Al-Azhar University Engineering Sector, vol. 19, pp. 25 - 50, 2024.

Received: 3 October 2023

Revised: 25 November 2023

Accepted: 3 December 2023

DOI: 10.21608/auej.2023.242261.1447

ABSTRACT

The current study aims to produce and design high-strength alkali-activated concrete (AAC), containing carbon fiber (CF) and the optimum content of waste brick powder (WBP) as source materials. A response surface method (RSM) was empolyed to design and optimize the properties of AAC. Three main parameters selected for this study were WBP content, Na_2SiO_3/KOH ratio, and CF content. Seventeen AAC mixtures were generated by activating the source materials with an alkaline-activation solution of KOH and Na_2SiO_3. The fresh properties, compressive, flexural strengths and density of the AACs were evaluated. The fresh AAC mixtures containing less than 40% WBP were highly workable with a diameter of 195–215 mm. The compressive, flexural strengths and density responses ranged from 22 and 121.22MPa, from 2.10 and 9.6MPa and from 2116 to 2366 kg/m^3. From expermental work, the optimum mix of WBP (5%), Na_2SiO_3/KOH ratio (1.90), and CF (1.0%) was found to develop the AAC with the optimum of WBP. According to microscopic investigation, the optimum mixture had a nonporous and dense microstructure compared other mixtures incorporated with WBP, which had best mechanical properties (111.15MPa, 8.3MPa and 2316kg/m^3). Finaly, it is possible to produce high strength AAC (70 MPa) with 40% waste brick powder content.

KEYWORDS: Waste brick powder, Microstructure, Response Surface Methodology-Compressive strength.

الخصائص الميكانيكية والبنية المجهرية للخرسانة المنشطة قلويا عالية المقاومة المحتوية على كميات كبيرة من بودرة الطوب استخدام منهجية سطح الاستجابة

صلاح خالد الخرينج*، محمد جمال مهدي، أحمد محمد طهوية

قسم الهندسة الانشائية، كلية الهندسة، جامعة المنصورة، جمهورية مصر العربية

***البريد الاليكتروني للباحث الرئيسي:** mng_salah@outlook.com

الملخص

تهدف الدراسة الحالية إلى إنتاج وتصميم الخرسانة المنشطة القلوية عالية المقاومة والتي تحتوي على ألياف الكربون والمحتوى الأمثل من مسحوق مخلفات الطوب كمواد أولية. تم استخدام منهجية سطح الاستجابة لتصميم وتحديد الخواص المثلي للخرسانة المنتجة. تم اختيار ثلاثة معايير رئيسية لهذه الدراسة وهي محتوى بودرة كسر الطوب ونسبة سيليكات الصوديوم الي هيدروكسيد البوتاسيوم ومحتوى الياف الكربون. تم تصميم وتنفيذ سبعة عشر خلطة خرسانية عن طريق تنشيط مواد المصدر بمحلول من هيدروكسيد البوتاسيوم وسيليكات الصوديوم. تم تحديد الخواص الطازجة ومقاومة الضغط والانحناء وكثافة الخرسانة المنتجة.

أظهرت النتائج التجريبية أن خلطات الخرسانة المنتجة الطازجة المحتوية على أقل من 40٪ WBP كانت فعالة للغاية بقطر 195-215 مم. تراوحت مقاومة الضغط ومقاومة الانحناء وكثافة الخلطات من 22 و122 ميجا باسكال، من 2.1 و9.6 ميجا باسكال ومن 2116 إلى 2366 كجم / م3 على التوالي. وقد وجد أن المزيج الأمثل مكون من (5% مسحوق مخلفات الطوب) ، ونسبة سيليكات الصوديوم الي هيدروكسيد البوتاسيوم (1.90)، ونسبة الياف الكربون (1.0%). ووفقا للفحص المجهري، فإن الخليط الأمثل له بنية مجهرية كثيفة وغير مسامية مقارنة بالخلطات الأخرى والتي كانت لها أفضل الخواص الميكانيكية (مقاومة الضغط 111.15 ميجاباسكال ومقاومة الانحناء 8.3 ميجاباسكال وكثافة الخرسانة 2316 كجم/م3). اثبتت النتائج انه يمكن انتاج خرسانة منشطة قلويا باستخدام بودرة كسر الطوب بنسبة 40% واعطت مقاومة ضغط 70 ميجاباسكال. هذ النوع من الخرسانة يخدم قطاعي البناء والتشييد والهندسة المدنية بشكل كبير ويقلل من المشاكل البيئية عن طريق إعادة تدوير مخلفات البناء.

الكلمات المفتاحية: بودرة مخلفات الطوب، البنية المجهرية، منهجية سطح الاستجابة، مقاومة الضغط.

1. INTRODUCTION

Recent national and international environmental laws and regulations have had a considerable impact on the Portland cement (PC) industry's use of natural raw materials, energy consumption, greenhouse gas emissions, and sustainability. As a result, as compared to PC mixes, alkali activated concretes (AACs), a crucial option for cementitious systems, can lower emissions and energy use [1]. AACs, which combine aluminosilicate materials and alkali activator solutions to create materials like ceramic structures, can replace PC [2, 3]. A range of natural raw materials, including some derived from production waste, can be used to make aluminosilicate materials. The employment of these aluminosilicate materials, such as fly-ash (FA) and slag (GGBS), is therefore becoming more significant in the construction industry. To create hybridization alkali-activated materials and better understand the properties of waste alkali-activated binders, numerous experiments have been carried out recently [4, 5].

The three aluminosilicate materials that are most frequently used in the manufacturing of AACs are FA, slag (GGBS), and metakaolin (MK) [5]. Two of these industrial byproducts that serve as a substitute for sustainable building materials are FA and GGBS. When the substance is activated in AACs, a C-S-H gel is created because of the high CaO concentration (> 30%) of GGBS and FA [6]. But alkalis' activation of FA and GGBS leads to the development of amorphous inorganic polymers. The primary parameters influencing the characteristics of the AACs are the chemical, mineralogical, and morphological characteristics of FA and GGBS, the type of alkali-activator solution (AAS), and the curing regimes. Particularly when compared to FA-based AAC, the degree of reaction is greater in GGBS-based AAC at both low and high temperatures [6-8]. It has been shown that under heat curing conditions, a denser structure occurs from an increase in reaction intensity and kinetic energy [8, 9]. Additionally, to make alkali activated binders, silicate- and oxide-based solutions are often used separately as alkali activator solutions [3,10-12]. Occasionally, the usage of NaOH and Na_2SiO_3 (SS) both significantly improve AAC's performance [11, 12].

A previous study [13] found that using both NaOH and SS solutions instead of simply the NaOH solution increased the 1-day strength of the AAC mixture from 40-90 MPa. The AACs are manufactured with the aluminosilicate materials (GGBS, FA), and the activators NaOH and SS under different curing regimes [9, 20]. The main factors, including the precursor content, alkali activation dose, type, precursor to fine aggregate, and water to precursor ratio need to be considered, which makes the mixture proportion design become more different compared to cement concrete. Additionally, to improve the mechanical characteristics of brittle composites, particularly tensile and shrinkage [16,17], short fibers are frequently incorporated. With the addition of short fiber, AAC composites exhibit notable gains in mechanical and durability properties [18, 19]. Different fiber types used in AAC composites have improved freezing thaw resistance and decreased shrinkage [20, 21]. Fibers made of steel, PE, PVA, PP, glass fibers, and carbon can be employed to produce AACs [18-20]. The employment of carbon fibers (CFs) for this purpose is not widely understood. Alkali-activated metakaolin [3], fly ash [5], and GGBS [22] were utilised as short carbon fibers in earlier research. Additionally,

research has been done on the production of AACs using waste glass, ceramic, and brick. For example, the efficacy of the AACs manufactured from brick powder has been examined [23]. In a different work, 3 distinct kinds of construction & demolition (C&D) waste were mixed with NaOH and SS solutions to produce alkali activated mortars [23, 24]. The mechanical and thermal properties of an AACs produced from ceramic waste were also examined [25]. In addition, the production of large amounts of brick waste (WB) during the manufacturing process and the demolition and construction processes has become an environmental and economic issue, and therefore it is advisable to recycle them in a good way to protect the environment and promote sustainability. As a result, various studies [17, 26] have investigated the possibility of using WB in the building and construction sector. AAC based on brick waste with a 2.0 SiO_2/Na_2O ratio and a 7 M NaOH molarity was developed [27].

Recent research [17, 24] investigated an effective optimal design technique for producing AAC and determining the best component parameters. Engineering data was described and analyzed using the response surface methodology (RSM), which employs statistical and mathematical techniques. RSM can decrease the number of labs. trials and improve the interactions between reaction component parts [28-30]. Via RSM, Aydn [22] found that AAC had the optimal FA and SF content. The RSM was also used by Revathi et al. [31] to examine the silica fume on FA-based alkali-activated mortars. Utilising RSM, Gao et al. [32] investigated the AAC mixture design and early compressive strength. RSM was used to optimize AAC in several studies [33-36].

Various techniques have been used to utilize waste brick as a source of aluminosilicates in the development of AAC, but with a high volume of WBP, the effect of KOH/SS ratios, and carbon fiber content, the application of any of the kinds of mix design to optimize their proportions has not been examined. The object of this design is to apply the RSM to designing and optimizing the manufacturing of high-strength alkali-activated concrete with a high-volume of WBP. The selected response of central centroid design (CCD) comprises generating models correlating compressive and flexural strength responses as dependent on the chosen variables. So, the target of this work is to get the highest strength performance possible, which can be achieved as a function of the selected variables. The mathematical models were developed using the experimental data and were statistically assessed by ANOVA and diagnostically validated. The best component domains from the selected variables were then selected using the response curves and the desirability function to create an optimized AAC with the maximum mechanical properties. Finally, the microstructure of the optimum mixtures was investigated by SEM and thermogravimetric analysis analyses.

2. EXPERIMENTAL STUDIES

2.1. Materials

In this investigation, AAC mixes were made using SF and GGBS, which complied with ASTM-C618 and ASTM-C1240. The GGBS has a coefficient of basicity of 1.86 and a modulus of hydration of 1.03, respectively. The GGBS and SF had a surface area of 392 m^2/kg and 23300 m^2/kg, respectively. The waste brick powder (WBP) which obtained by brick processing and construction and demolition waste. It was crushed and sieved to get WBP. WBP was employed to partially substitute GGBS as a precursor in AACs production. Fig. 1 showed SEM micrographs of used source materials. It is found from that slag has an irregular shape, while SF has a spherical shape with tiny particles. The WBP particles were also found irregular shape despite the surface being smooth. The particle size distributions (PSDs) of the WBP and other materials was presented in Figs. 2 and 3. It was noticed that the WBP particles is comparable of GGBS particle. Table 1 presented the oxides composition of the WBP particles and raw materials as determined using X-ray fluorescence.

In the current study, natural sand (NS) was used as fine aggregate. NS with a fineness modulus of 2.56 in the range of 0/0.4 mm was used. The used fine aggregates were agreed with BS EN 12620/2002.

Carbon fiber size and aspect ratio are critical criteria that influence the improvement of concrete's mechanical properties [23, 24]. According to trials and previous studies, carbon fibers (with a length of approximately 6 mm and a diameter of approximately 7 μm) were utilized in this study to create the AASM samples. Table 2 displays specific details concerning carbon fibers.

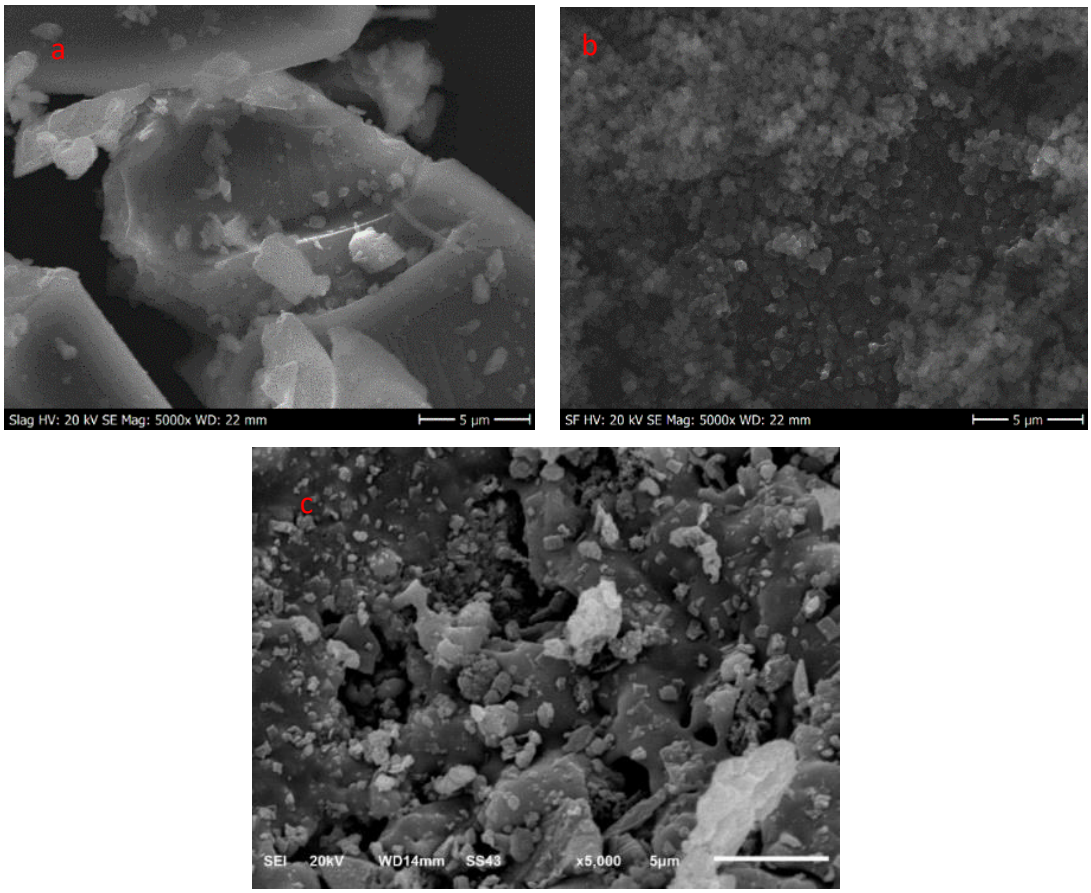

Fig. 1. SEM micrograph of source materials a) GGBS, b) SF, and c) WBP.

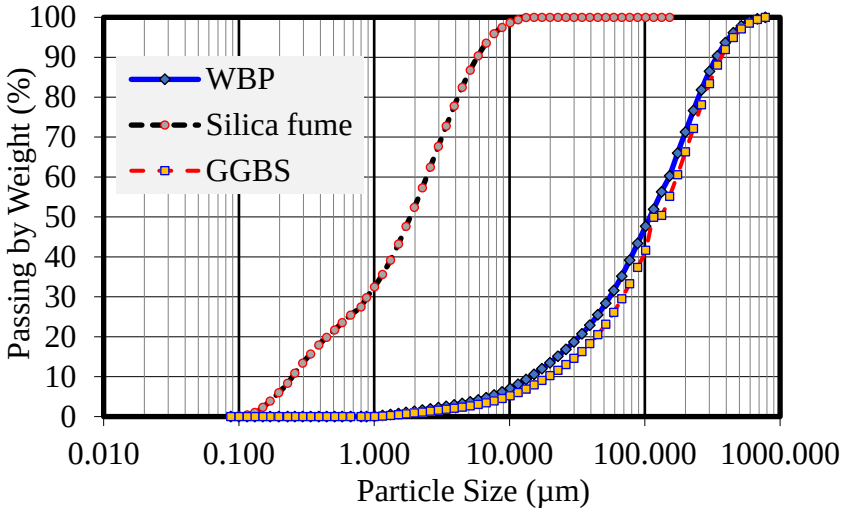

Fig. 2. PSD of source materials.

Fig. 3. The picture of WBP.

Table 1. Oxides of GGBS, SF, and WBP (%).

Oxides	Slag	SF	WBP
SiO_2	41.6	98.8	83.34
Al_2O_3	13.96	0.22	1.4
Fe_2O_3	1.49	0.14	0.2
MgO	5.53	0.3	2.39
CaO	34.53	0.12	7.28
Na_2O	0.49	0.01	5.39
K_2O	0.97	0.21	-
ZnO	0.01	0.1	-
S^{2-}	1.42	-	-
LOI	1	2.7	-

Table 2. Main parameters of carbon fiber

Fiber diameter (μm)	Length (mm)	Tensile strength (GPa)	Elastic modulus (GPa)	Density (g/cm^3)	Electrical resistivity Ω.cm
7.0	6.0	3.1-3.7	220-235	1.78	$4.58\ 10^{-3}$

2.1.1. Matrix production and preparation

According to the trail experimental mixtures, the author designed the high-strength alkali-activated concrete. The prepared alkali-activated concrete is composed of GGBS and SF as precursors, and KOH and Na_2SiO_3 are the alkali-activated materials. Therefore, the authors tried to develop this concrete type with new parameters such as carbon fiber, WBP, KOH, and Na2SiO3 ratio. The AAC mix design method includes three steps: 1) evaluate optimum WBP content; 2) define a SS/KOH ratio; 3) evaluate the optimum carbon fiber content. The control mix is made up of slag and silica fume as aluminosilicate materials. The control mix was constructed and prepared with GGBS in multiple tests for the development of AAC mixtures, with SF substituted at a fixed ratio of 25% by slag mass. The reason for fixing the silica fume ratio was to conduct experimental mixtures without any other aluminosilicate materials, and it was noted that the mechanical properties were the best possible at this ratio. All series were carried out based on the proportions of the control mix. The extra water and fine aggregate content were content in all mixtures. Hobart blender used for the AAC

manufacturing has a 140 r/min planetary motion. SS and KOH were combined in a specific ratio to produce the alkali activator solution (AAS), which was made the day before. To prepare the AAC, for two minutes the solid ingredients were mixed in dry case. Then, addition of AAS and mixed for 2.5 min. Eventually, the CFs were evenly introduced in the mortar and continuously blended for another 2.5 min to ensure an effective distribution. The fresh matrix was then quickly covered with a plastic sheet, leaving no room for air to escape to prevent water loss. The mixture was then allowed to cure for 24 hours at lab. temperature in the moulds. The samples were then taken out of the moulds once they had solidified, and they were naturally cured for a further 48 hours at 65 oC before being characterized. The synthesis combinations of the AAC are detail presented in Table 2.

2.1.2. RSM and Experimental Works

In the current study, three main parameters were selected (WBP content, alkali activator concentration, and CF content). Various mix components were performed by adopting central composite design via RSM. This method was used in 17 mixtures, using 5-center points for error calculation and a set of points located at the midpoint of each edge. Seventeen AAC were generated by activating the source materials with an AAS of KOH and waterglass. Table 3 lists the different independent variable codes and levels that were examined. RSM is a very effective method. Because RSM uses a partial factorial design, fewer experiments are needed. The 2k factorial and simplex designs are the most popular first-order designs, but the CCD methods are the most popular second-order designs. RSM focuses on the connections between factors and results. Examining the influences of individual factors and parameter interactions on response variables may be done using the proposed model. With just a few trial data points, the RSM can create a strong model, concentrate on parameter interactions, and pinpoint the ideal solution.

The most important RSM is CCD, which consists of three groups of design points (Fig. 4) :at the cube's vertices, two-level factorials are used to represent all possible mixtures of the (+1 and -1) coded values. The axial-points, which are positioned at a distance from the center of each cube face in the practical experiment area, allow for rotation. For the center-points, which are in the cube's center, each variable's coded value is set to 0.

As a result, AAC mixtures were produced utilizing the RSM method and the Design-Expert® software design tool. These design considerations and their associated results are used to evaluate the second order-polynomial model for each response using equation (1):

$$y = \beta 0 + \sum \beta_i x_i + \sum \beta_{ii} x_i^2 + \sum \beta_{ij} x_i x_j \quad (1)$$

where y is the expected response, β0 denotes the model's intercept, βi denotes linear coefficients, βii denotes quadratic coefficients, βij denotes the coefficients of variable interaction, and xi, xj denote independent variables like those in Tables 3 and 4.

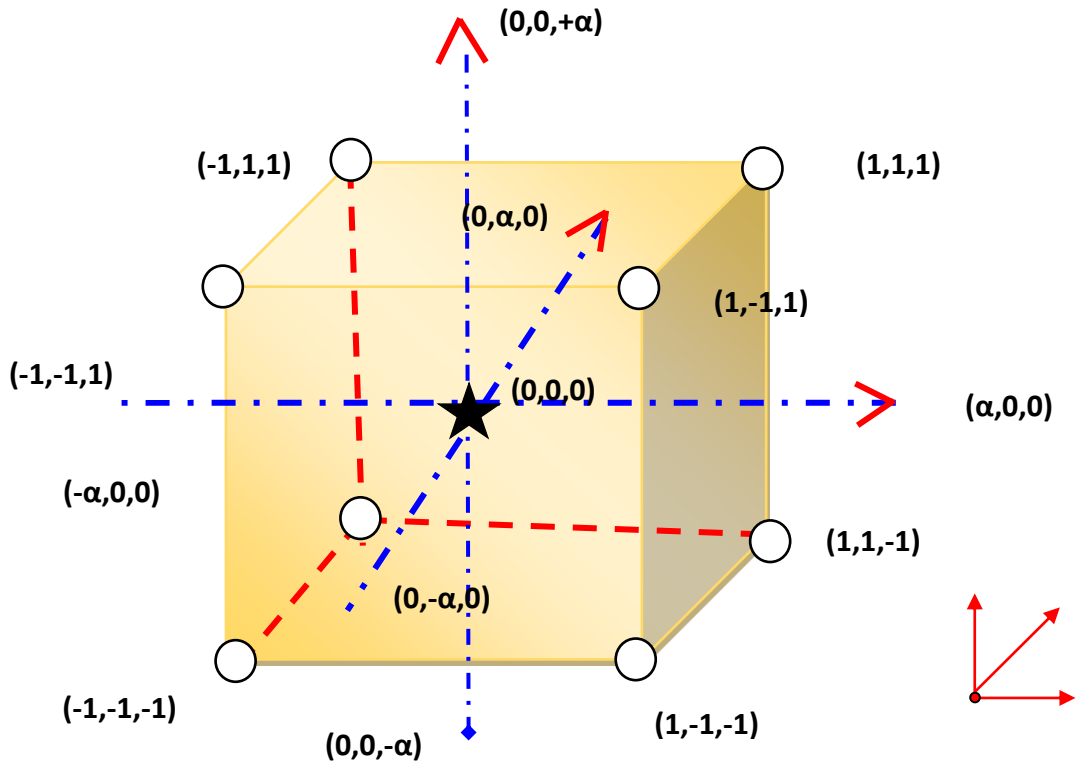

Fig. 4. A CCD method.

Table 3. Experimental mixtures design of AAC (kg/m³).

Mixtures	Source materials			Natural Sand	AAS		SS/KOH ratio	Extra water	Carbon fiber	
	GGBS	SF	WBP		KOH	SS			Kg/m³	%
M1(Control)	674	170	0	1135	62	186	3	79	0	0
M2	404		224			93	1.5		9	0.5
M3	404		224			186	3		18	1
M4	135		448			186	3		9	0.5
M5	135		448			0	0		9	0.5
M6	404		224			93	1.5		9	0.5
M7	674		0			186	3		9	0.5
M8	404		224			93	1.5		9	0.5
M9	404		224			93	1.5		9	0.5
M10	404		224			0	0		0	0
M11	674		0			93	1.5		18	1
M12	135		448			93	1.5		0	0
M13	404		224			0	0		18	1
M14	404		224			93	1.5		9	0.5
M15	135		448			93	1.5		18	1
M16	404		224			93	1.5		9	0.5
M17	404		224			186	3		0	0

Table 4. Limits/coded value of independent variables.

Varia.	Code	Maximum & Minimum levels		
		-1	0	+1
A (SS/KOH ratios) (Unitless)	A	0	1.5	3.0
B (WBP) (%)	B	0	40	80
CF (%)	C	0	0.50	1.0

2.2. Test Methods

2.2.1. Fresh properties.

The workability test was performed based on ASTM C1437. A little cone droop received the addition of the new mixture. The average of the largest and least slump was used to determine the slump of the new mixture. Based on plasticity change caused by physical and chemical reactions in the raw materials, the manual Vicat needle was used to compute the AAC setting time. According to ASTM C807-21 standard, the setting time of fresh mortar during the initial stage was measured every 60 s.

2.2.2. Compressive and flexural strengths

The cubic samples (5.0 x 5.0 x 5.0 cm) underwent uniaxial compressive testing to ascertain the compressive strength. The compressive test was carried out at a loading rate of 2.1 kN/s until the sample failed using a universal apparatus with a maximum load of 500 kN. Three-point flexural testing in accordance with ASTM C348-21was performed on prism sample (40 x 40 x 160 mm) to ascertain the flexural strength. For the optimized mixes, the strength and bulk density were also assessed after 28 days.

2.2.3. Microstructure tests

A SEM test was done to investigate the synthesized AAC as well as the raw materials used in the technique. The investigation was performed using a Jeol JSM 6610 FESEM. Using a Netzsch STA 449C thermal analyzer, TGA measurements were performed under conditions of 8 °C/min. The nitrogen was added to create a steady environment. To stop the reaction and assure TGA test quality, the hardened AAC samples were broken into pieces that were approximately 5 × 5 × 5 mm in size and submerged in 100% ethyl alcohol for at least 7 days.

3. Results and discussion

3.1. Response analysis of 1 day and 28 days strength

The 1-and 28-days compressive strength (CS) responses of AACs are shown in Table 5 together with experimental and predicted values as well as absolute relative deviations (RD) based on the experimental design parameters. Table 5 evaluated the model's reliability of several kinds of fitting equations for the link between the outcomes of the mechanical strength and the independent parameter. The statistical analysis's description of the significance of the misfit and hypothesis test analyses employed the letter P. While 0.01 > P 0.05 and P > 0.05 were regarded as significant and not significant, respectively. There were no mismatches and the quadratic model of one day's CS adequately fit the true data (P = 0.0011, modified R^2 = 0.9367). The quadratic's P-value in the 28-day compressive strength model was 0.0005. Hence, the quadratic model in this test characterized the link between the response parameter and the major effects. The critical components that influence CS at 1-day and 28 days of curing are listed in the following order of magnitude: B > A–C. The fully quadratic polynomial model needs more research before being used in subsequent studies.

Table 6 also contains the reliability test results for Models $C.S_{1d}$ and $C.S_{28d}$. The model's excellent dependability and accuracy were shown by the coefficient of variation values being less than five percent and the signal-to-noise ratio values being both larger than 4 as recommended by

[35,41]. Moreover, Eqs. (1) and (2) are produced by multiplying the chosen coefficients by the equation for compressive strength (C.S) of the totally quadratic polynomial.

$$C.S_{1d} = +50.57 +12.79\ A -26.97\ B+1.35C -10.53AB+0.0001\ AC-1.09\ BC-8.08A^2 +4.43\ B^2 +6.49\ C^2 \quad (1)$$

$$C.S_{28d} = +63.21 +15.99\ A -33.71B +1.68\ C -13.16AB +0.0001AC-1.36\ BC-10.10\ A^2+5.53\ B^2 +8.11\ C^2 \quad (2)$$

The relationships between the dependent and independent parameters could be presented in a contour plot by jointly creating analogous surfaces (Figs. 5,6, and 7). For instance, Fig. 5 shows the influences of the ratio of the SS/KOH and waste brick powder (WBP) concentrations without the addition of carbon fiber (0 levels). The compressive strength after one day of curing increased considerably and peaked at roughly with an increase in alkali activator concentration ratio (SS/KOH ratio of 3). This is due to a higher alkali-activated concentration leads to a rise in the alkali system reaction, which results in a significant amount of starting materials dissolution. The positive effects of the alkali content (SS/KOH ratio of 3) on the performance of the AAC are agreed with the results of [2,10], in contrast to the negative effects of a waste brick powder (WBP) concentration level, which have been extensively documented, such as by [23], and Hwang et al. [42]. Fig. 6 illustrates the influences of the ratio of the CF and WBP concentrations at SS/KOH ratio of 1.5. It was demonstrating that carbon fiber concentration significantly increased the CS after one day of curing. Up to 1% by volume of carbon fiber can result in a better strength value, showing that the addition of some carbon fiber can enhance the performance of alkali-activated slag materials, particularly at high alkali activator concentrations. A recent paper by [42,43] also shown that alkali materials have a high volume of waste brick that enhances the material's structure and produces brittleness with microcracks. Finally, the interaction between the WBP and alkali activator concentration in Fig. 7 illustrates the effects of the ratio of the carbon fiber and SS/KOH ratio at waste brick powder (WBP) content of 40%. This response had a contour line that was essentially circular. The relationship between the two components was significant and reached a maximum value since the response surface is convex and only has one side.

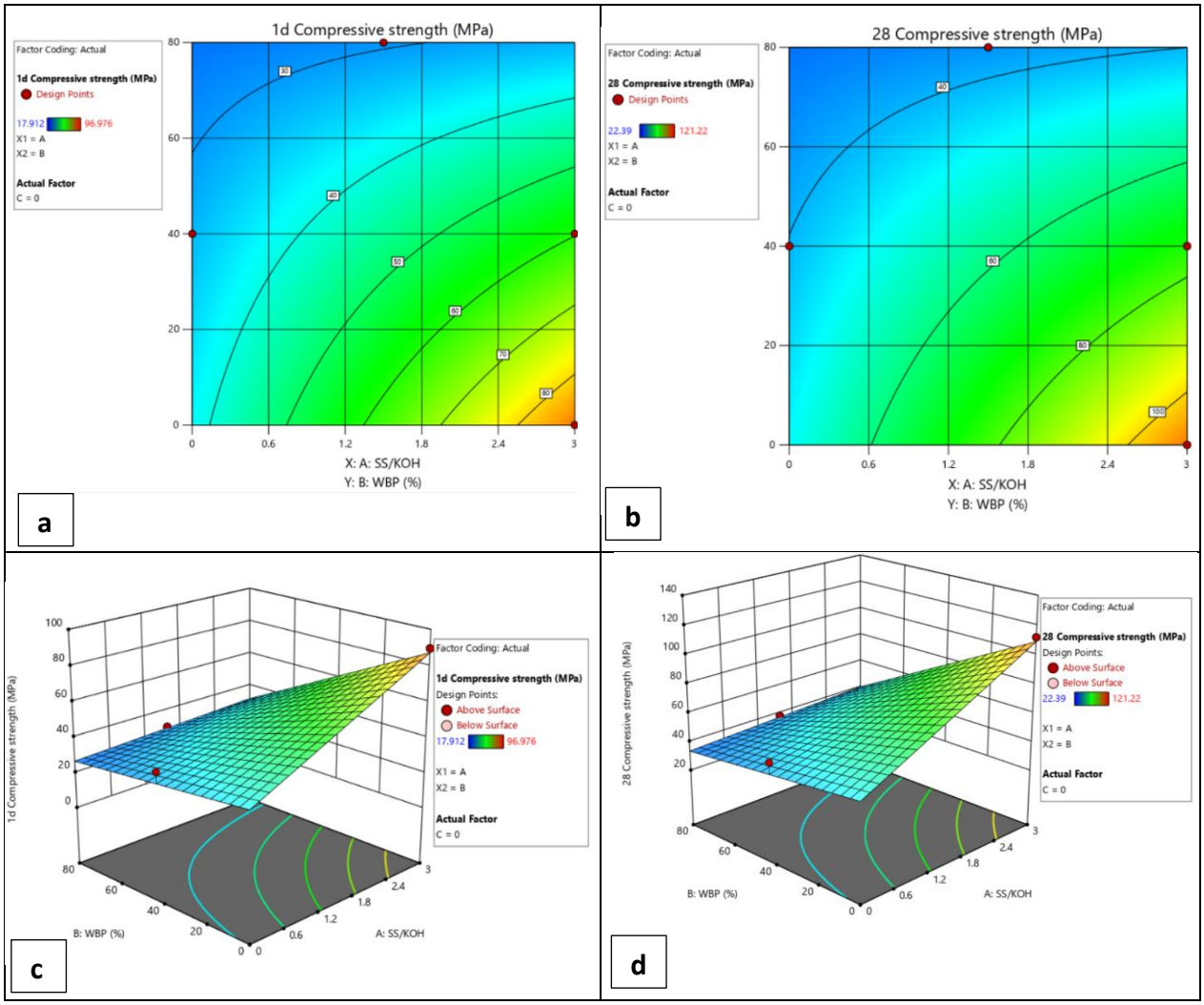

Fig. 5. The relationship of the two parameters on 1-d and 28-day compressive strength at 0% carbon content a) CS of 1-d , b) CS of 1-d, c) 3D contour for 1-day compressive strength, d) 3D contour for 28day compressive strength.

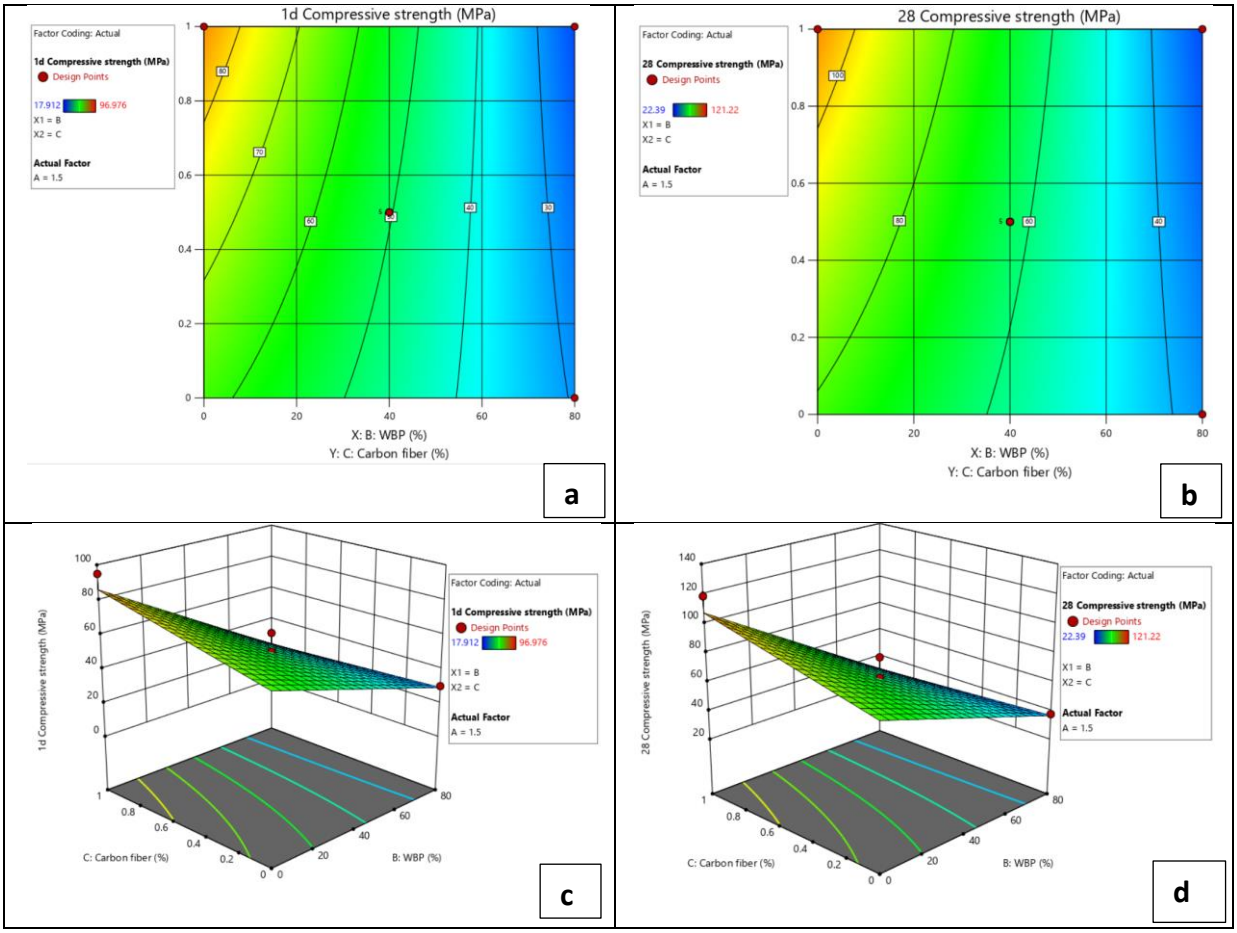

Fig. 6. The relationship of the two parameters on 1-d and 28-day compressive strength at solution concentration of 1.5 a) CS of 1-d , b) CS of 1-d, c) 3D contour for 1-day compressive strength, d) 3D contour for 28day compressive strength.

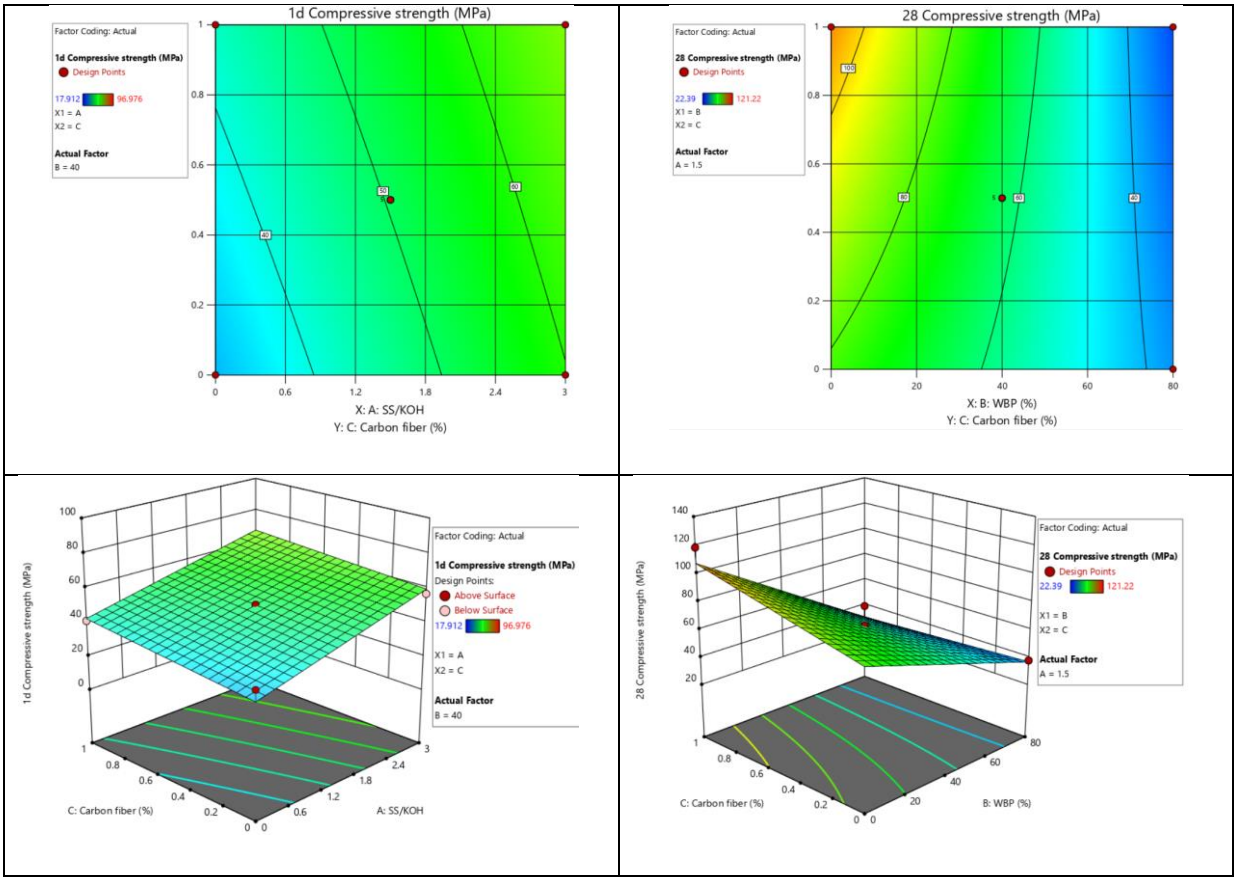

Fig. 7. The relationship of the two parameters on 1-d and 28-day CS at 40% content of WBP) CS of 1-d , b) CS of 1-d, c) 3D contour for 1-day compressive strength, d) 3D contour for 28day compressive strength.

Table 5. The experimental and predicted results of CS for the AAC mixtures.

Mixtures	Independent Variables			1d C.S (MPa)			28d C.S (MPa)		
	A	B (%)	C (%)	Exper.	Pred.	RD	Exper.	Pred.	RD
M1(Control)*	3.0	0	0	89.78	88.01	1.97	112.22	110.78	1.28
M2*	1.5	0	1	94.94	92.94	2.11	118.67	117.04	1.37
M3*	1.5	40	0.5	50.57	49.40	2.31	63.21	62.31	1.43
M4	1.5	80	1	31.01	30.39	2.01	38.76	38.25	1.31
M5*	3.0	0	0.5	96.98	94.05	3.02	121.22	118.90	1.91
M6	0	40	0	38.66	37.48	3.06	48.33	47.40	1.93
M7	1.5	40	0.5	50.57	49.18	2.74	63.21	62.12	1.73
M8	0	0	0.5	42.97	41.97	2.32	53.71	52.93	1.46
M9	0	80	0.5	17.91	17.53	2.12	22.39	22.09	1.34
M10	3.0	80	0.5	29.80	28.58	4.11	37.25	36.28	2.61
M11*	3.0	40	0	56.89	55.39	2.64	71.11	69.92	1.67
M12*	1.5	40	0.5	50.57	49.29	2.53	63.21	62.20	1.59
M13	0	40	1	41.06	40.07	2.41	51.33	50.55	1.52
M14	1.5	80	0	30.21	29.64	1.89	37.76	37.31	1.19
M15*	3.0	40	1	59.29	57.30	3.36	74.11	72.53	2.13
M16	1.5	40	0.5	50.57	48.36	4.37	63.21	61.47	2.76
M17	1.5	40	0.5	50.57	49.46	2.19	63.33	62.14	1.37

3.2. Response surface analysis of flexural strength and unit weight

The mixture design containing WBP, carbon fiber, and alkali activated concentration and the responses (flexural strength and unit weight) of each AAC are presented in Table 5. The flexural strength and unit weight of the AAC samples varies in the ranges of 2.10 and 9.6 MPa and from 2116 to 2366 kg/m3, respectively. The mixtures with WBP of 40% or more (M4, M9, M10 and M14) had lower unit weight and flexural strength than the control mixture (M0). Additionally, a significant relation was found between these two responses ($r = 0.96$; p-value < 0.001), as indicated in the previous studies. The physicochemical measurements will eventually be used to interpret the collected data. The major impact of the regression was statistically significant, according to the analysis of variance data in Table 6, where the p-value risk significance probability was below 0.05.

Table 6. The experimental and forecast results of the AAC mixtures at 28 days.

Mixtures	Independent Variables			Flexural strength	Unit weight
	A	B (%)	C (%)	MPa	kg/m^3
M1(Control)*	3.0	0	0	7.02	2358
M2*	1.5	0	1	7.9	2304
M3*	1.5	40	0.5	6.1	2230
M4	1.5	80	1	3.6	2164
M5*	3.0	0	0.5	9.6	2366
M6	0	40	0	4.1	2186
M7	1.5	40	0.5	5.9	2231
M8	0	0	0.5	4.9	2256
M9	0	80	0.5	2.1	2116
M10	3.0	80	0.5	3.5	2188
M11*	3.0	40	0	5.6	2279
M12*	1.5	40	0.5	5.9	2230
M13	0	40	1	4.9	2192
M14	1.5	80	0	2.9	2160
M15*	3.0	40	1	6.3	2286
M16	1.5	40	0.5	5.9	2231
M17	1.5	40	0.5	5.9	2232

Table 7. Analysis of variance for the fitted model.

Response	Source	Sum of Squares	df	Mean Square	F-value	p-value	R^2
1d Compressive strength	Mean vs Total	45794.28	1	45794.28			0.932
	Linear vs Mean	7342.81	3	2447.6	32.24	< 0.0001	
	2FI vs Linear	633.54	3	211.18	5.97		
	Quadratic vs 2FI	178.32	3	59.44	2.37		
	Cubic vs Quadratic	175.2	3	58.4			
	Residual	0	4	0			
	Total	54124.15	17	3183.77			
28d Compressive strength	Mean vs Total	71569.13	1	71569.13			0.931
	Linear vs Mean	11472.92	3	3824.31	32.24	< 0.0001	
	2FI vs Linear	**989.7**	**3**	**329.9**	**5.97**		
	Quadratic vs 2FI	278.68	3	92.89	2.38		
	Cubic vs Quadratic	273.73	3	91.24	31682.14	< 0.0001	
	Residual	0.0115	4	0.0029			
	Total	84584.17	17	4975.54			
Dry Unit weight	Linear vs Mean	72793.93	3	24264.64	525.27	< 0.0001	0.99
	2FI vs Linear	**375.79**	**3**	**125.26**	**5.57**		
	Quadratic vs 2FI	53.06	3	17.69	0.721		
	Cubic vs Quadratic	168.89	3	56.3	80.42		
	Residual	2.8	4	0.7			
	Total	8.51E+07	17	5.00E+06			
Flexural Strength	Mean vs Total	499.18	1	499.18			0.962
	Linear vs Mean	**47.64**	**3**	**15.88**	**27.93**	**< 0.0001**	
	2FI vs Linear	2.15	3	0.7168	1.37		
	Quadratic vs 2FI	**3.19**	**3**	**1.06**	**3.61**		
	Cubic vs Quadratic	2.02	3	0.6747	84.34		
	Residual	0.032	4	0.008			
	Total	554.21	17	32.6			

3.3 Validation of ANOVA models

It's interesting that before being employed, the ANOVA-models created in this paper. The comparison between the anticipated R^2 and adjusted R^2 for each answer, as presented in Table 8, was less than 0.2, showing that they are logically consistent [31], [44]. The generated model was approved, and the correct precision for each response was more than 4. Table 8 and 9 displays the ANOVA results for the whole regression model of all responses. The models are important when the F-value is larger and the probability is lower, less than 0.005 [39], [45], [46]. Table 9 shows the experiment results and the forecasting models for the AAC mixture, which investigate which properties are the best in terms of both physics and mechanics. The experimental study confirmed that the mixtures had 5% WBP content, 1.9 SS/KOH ratio, and 1.0% carbon fiber content, which had a 216 mm flowability diameter, a dry unit weight of 2316 kg/m3, a flexural strength of 8.30 MPa, a 1d compressive strength of 83.74 MPa, and a 28d CS of 111.15 MPa.

Table 8. ANOVA results for responses.

Response	1d CS (MPa)	28d CS (MPa)	Dry density (kg/m^3)	Flexural Strength (MPa)
Standard deviation	4.94	4.80	4.74	1.59
Mean	50.44	2462.2	2232.6	5.98
Pred. R^2	0.932	0.9851	0.99	0.962
Adj. R^2	0.8921	0.915	0.881	0.8401
p-value	< 0.0001	< 0.0001	< 0.0001	< 0.0001

Table 9. Results of the experiment and forecasting results for optimal mix design.

Response	1d CS (MPa)	28d CS (MPa)	Dry density (kg/m^3)	Flexural Strength (MPa)
Predicted value	83.06	111.15	2316.0	8.30
Expr. value	83.74	112.13	2326.60	8.42
Deviation (%)	0.83	0.89	0.46	1.43

3.4. Properties of AAC containing WBP and Carbon fiber

According to the experimental results, compressive strengths of 25–120 MPa were recorded with an alkali activator concentration ranging from 0 to 3.0, a WBP content in the range of 0 to 80%, and a carbon fiber content in the range of 0 to 1% (vol.) at 65 oC for 48 h, and it was found that WBP may substitute up to 80% of GGBS. Hwang et al. [42, 43] and Rovnaník et al. [44]developed blended fly ash and slag alkali-activated mortars with brick powder. Alkaline solutions SS and KOH, as well as additional starting components GGBS and SF, were used to generate AAC including WBP [42, 45]. Therefore, seven samples are marked in Table 4 that tested to determine their strength, microstructure, and durability characteristics.

3.4.1. Workability and setting time.

The workability of AAC containing WBP is presented in Fig. 8, with diameter values for mixtures calculated in the 168-255 mm range. The workability analysis demonstrated that WBP produced highly workable mortars even though all the workability results were larger than 90 mm as recommended by ASTM C 1621/C1621M-06. Generally, the AACMs without WBP had better workability than the AAC with WBP. Moreover, the sag of the AAC was strengthened by the WBP's huge surface area and wildly irregular [42, 44]. The largest slump flow values were seen in the reference mixes (M1), which were then decreased by the addition of WBP, carbon fiber, and low concentration of alkali activated ratio. The slump flow of the AAC mixtures M3, M11, M12 and M15 was, respectively, 21.63%, 11.98%, 13.90%, and 6.05% lower than that of the reference mix (M1), which included 40% WBP. As the percentage of WBP increased and the alkali activated ratio (SS/KOH ratio) decreased, the workability was declined [44]. This is probably due to the hydrophobic property and physio-chemical properties of WBP, which lead to a decrease the moisture in mixtures. Nonetheless, at larger WBP concentration levels and carbon fiber, the effect was more pronounced. Finally, WBP is a less reactive powder than GGBS. WBP is a less reactive powder than GGBS, resulting to the reduction of the workability. Fig. 8b shows the setting times of AAC mortar and WBP-based mortar mixtures. The setting time of AAC mortar was in the range of 62 minutes to 27 minutes, whereas the setting time of WBP-based mixtures is shortened to 43 minutes to 23 minutes with the incorporation of WBP content and carbon fiber. It also was found that the alkali activator solution effect on the setting time. For example, the setting times of M2 were 53 min and 62 min, respectively, which have the highest setting times at low concentration of alkali activator (SS/KOH ratio of 1.5). contrarily, the M15 had the shorten setting times were 18 min and 23 min, respectively.

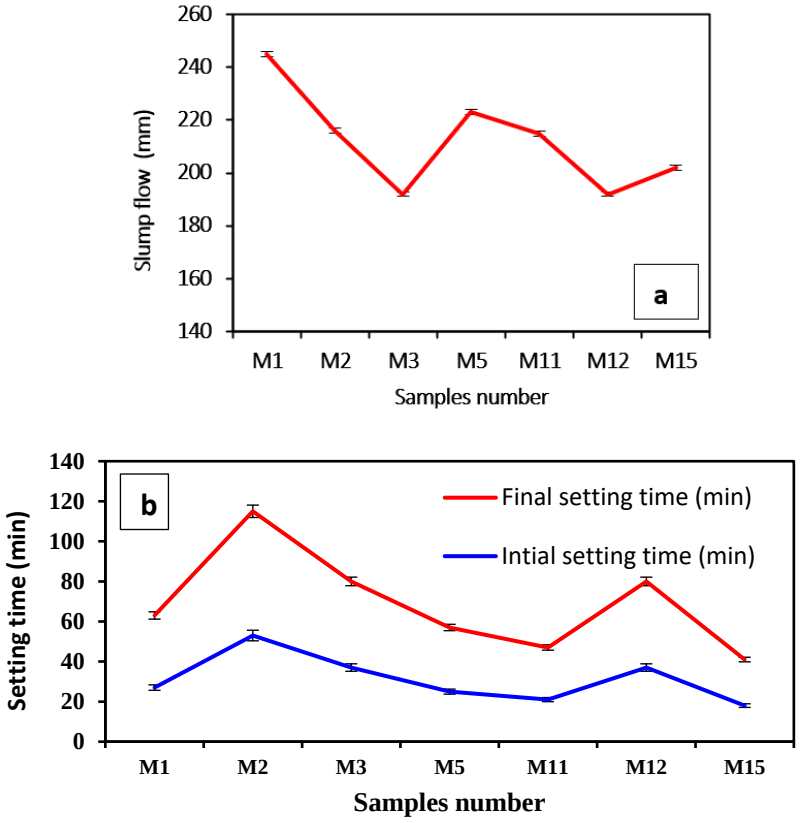

Fig. 8. a) Workability and b) setting times of WBP based- AAC with carbon fiber.

3.4.2. Compressive strength development

Fig. 9 shows the 1, 7, 28, and 90-day CS results for the AAC containing in the range of 0 to 40%WBP, demonstrating at 90-days of curing, CSs of 66–129 MPa were attained. The AAC compressive strength were frequently higher than those of mixtures that also included WBP. After 90 days of curing, M5 (containing 0.5% carbon fiber) had the highest strength, measuring 129 MPa, while M1 (the control mixture), with an alkali activated ratio of 3, had the lowest strength of 119 MPa. M12 (with 40%WBP and an alkali activated ratio of 1.5) displayed the lowest strength value of 66 MPa, whereas M11 measured at 76 MPa. At 90 days after curing, WBP-containing AAC samples had compressive strengths that were 39-51% lower than those of the control combination. It was discovered that GGBS had a median (d50) particle size that was 5.45 times coarser than WBP's. The pace of alkali activation process and gel formation, which can increase the mechanical strength of hardened mortars, may therefore be reasonably sped up as a result [42]. Furthermore, the alkali activation of each AAC mixture was impacted by the material compositions of WBP. Table 1 shows that the CaO content of GGBS is nearly 4 times higher than that of WBP. The formation of C(N)-A-S-H gels, may be facilitated by greater CaO concentrations in GGBS, as previously mentioned. These gels operate as additional glues to promote the alkali activation reaction. It was found that when the percentage of slag improved the strength values of all the combinations cured at heat curing increased as well. GGBS has a higher surface area and is extremely amorphous, accelerated the precursor material's reaction with the alkaline activator. Considering the increasing CaO concentration in the GGBS, a large amount of calcium ions leached into the reaction, which was rich in silicon and aluminum ions, during the hydration mechanism [18, 40, 43]. Increased GGBS content caused denser gel to develop, which eventually improved the mortar's compressive strength. Despite the failure of the 80% WBP samples to harden and set, a high strength AAC was created by swapping out 40% of the WBP powders for GGBS and the silica fume with using carbon fiber as shown in Table 6. This improvement was most likely made possible by the ternary binder impact of the WBP, silica fume, and GGBS alkali activation process when carbon fiber was present. Similarly, Fig. 10 showed the 7-d,28-d, and 90-day flexural strength results for the AAC containing in the range of 0 to 40%WBP, demonstrating that after 28 days of curing, flexural strengths of 5.0–9.0 MPa were attained. The effect of presence of carbon fiber on the AAC is significant in the improvement of flexural behavior. For example, the flexural strength of M5 at 28-day increased by 35% with the incorporation of 0.5% of carbon fiber compared to the M0. This enhancement in the strength attribute to the bridge role of fiber to reduce the crack width, these results is consistent with the previous studies [18-20,46]. Contrarily, the incorporation of WBP reduce the flexural strength as seen in the Fig. 10. This trend is agreed also with the compressive strength performance and agreed with [18,46].

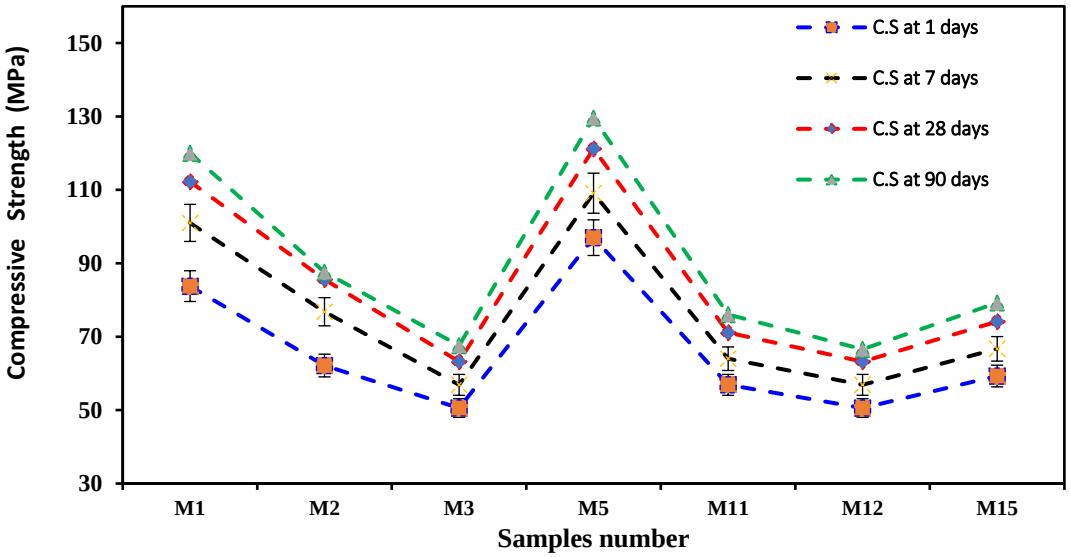

Fig. 9. Compressive strength WBP based- AAC with carbon fiber.

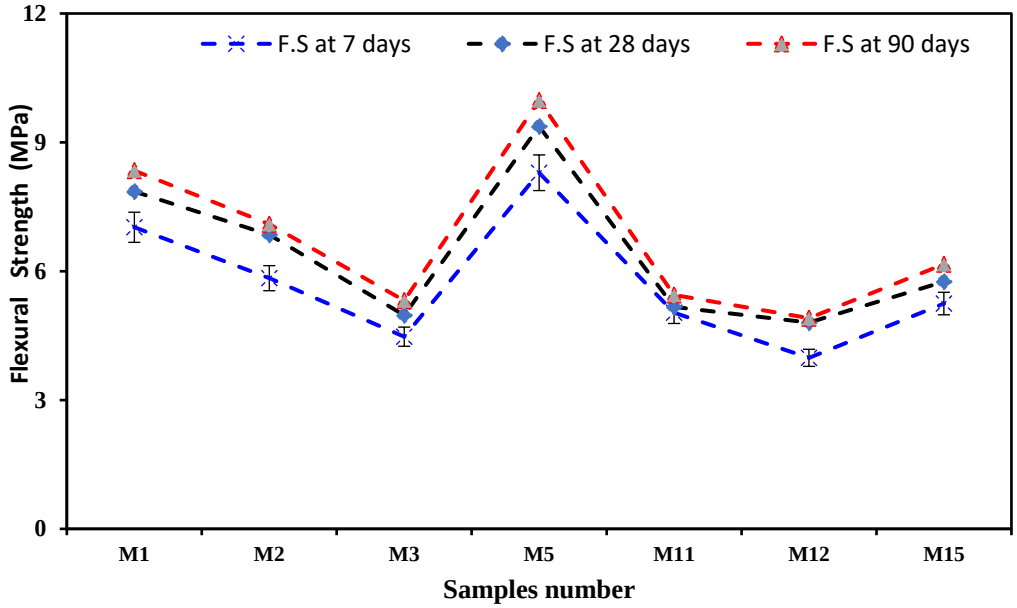

Fig. 10. Flexural strength WBP based- AAC with carbon fiber.

3.4.3. UPV test

The UPV test is an indirect indicator of mechanical and durability that evaluates modifications to concrete's properties, such as the development of C.S, and determines the degree of degradation or cracking in the mortars [42-44]. The results of the UPV test for the AAC are displayed in Fig. 11. After 90 days of cure, the data show UPV values ranging from 2.6 to 4.2 km/s. The results of the test dropped after 28-days, and all results of AAC samples increased with curing time. The findings of the 28-day UPV were 2.9-5.2% higher than the corresponding 1- and 7-day findings, and the experimental findings of the 90-day UPV were 1.9-3.1% higher than the corresponding 28-day values. The AAC mixtures displayed greater UPV values than the combinations containing WBP, as was to be predicted. As previously mentioned, GGBS has more surface area and CaO concentration than WBP, which speeds up the alkali activation reaction and creates more alkali activated gels that appear to decrease

porosity and enhance UPV. Also, as the amount of carbon fiber content rose, the UPV values gradually climbed. At 90-day ages, the M1 and M5 mixtures displayed 3.82 km/s and 4.21 km/s, respectively, whereas the M3 and M15 mixtures displayed 2.81 km/s and 3.09 km/s, respectively [43]. Further C-A-S-H and N-A-S-H gels eventually limit the hardened mortar's porosity, which is necessary for the development of a morphology density, an improvement in the strength of the AAC mixtures [42-44]. In addition, as WBP content increased in all the AAC samples, the UPV decreased. It appears that the improvement patterns for the UPV and CS results were comparable, rising with increases in GGBS content and curing time [45]. The relation between the C.S and UPV results of the AAC was then investigated using a linear regression, as depicted in Fig. 12. As predicted, there was a strong correlation between UPV and CS, with an R2 value of 0.96, according to the equation y = 44.429x - 59.495.

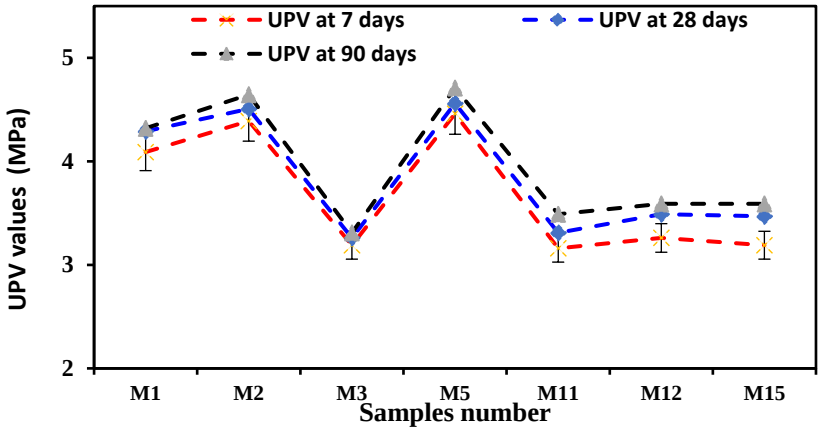

Fig. 11. UPV values of AAC samples.

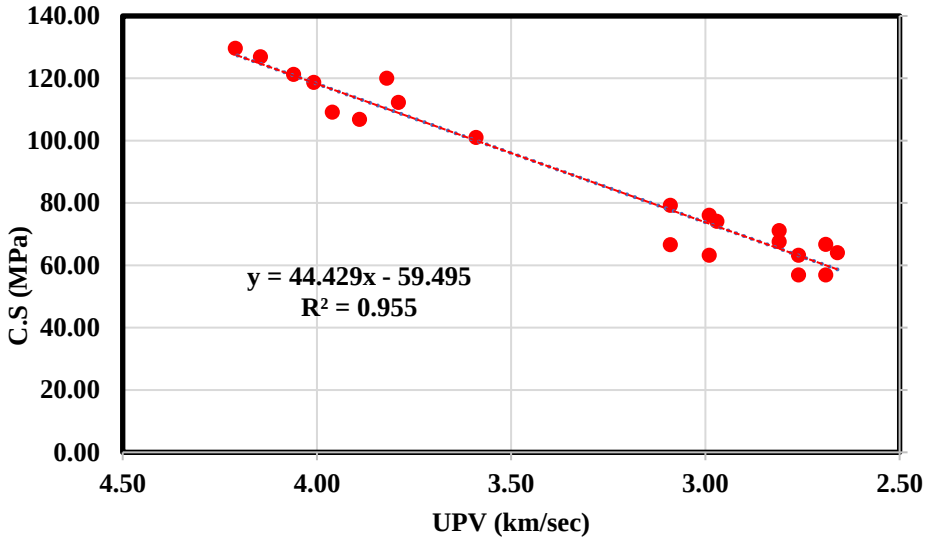

Fig. 12. The relation between C.S and UPV values of AAC samples.

3.4.4. TGA analysis

Fig. 13 shows the TG curves for selected AAC and WBP-based samples (M1, M5, M11, and M15) after 28 days of curing. It is found that the samples mass is gradually lose with the temperature increased. While the total weight loss similarly has a narrow range, between 5 and 9%, demonstrating that water is tightly bound in the hardened samples, the mass loss up to 200°C ranges between 3 and 6% and is related to the loss of free water. Therefore, in addition

to the favorable mineralogical composition of the raw materials, the apparent strength of these samples, ranging between 63 and 118 MPa, is also attributable to the proper water content present in the initial paste, which starts favorable reactions and leads to the formation of a dense structure [47, 48]. The control mixture, on the other hand, exhibits completely different behaviour despite acquiring a higher compressive strength (more than 100 MPa). The M5 achieved the lowest mass loss (5.13%), while the control mixture had 6% of mass loss. The role of WBP presence had a significant influence in the increasing of the weight loss reached 31.5% (M15) and 45.6%, (M11) higher than the control mix. These results agreed with the compressive strength and microscopic analysis, as well as similar results have been observed in earlier experiments [7, 43].

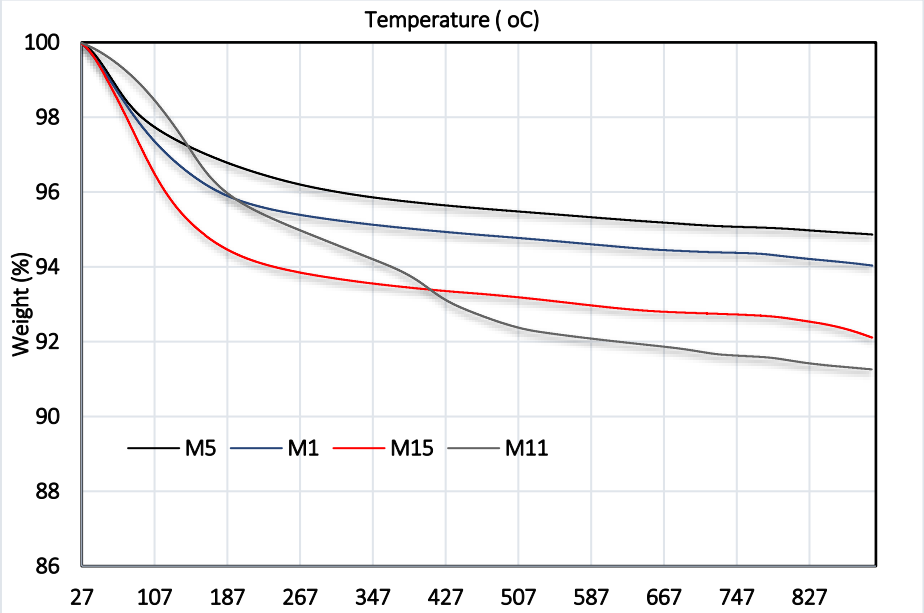

Fig. 13. TGA curves of selected samples produced from GGBS, WBP, and carbon fiber.

3.4.5. Microstructural observation

To examine the morphological and microstructural characteristics of selected 28-day cured AAC and WBP-based samples (M1, M5, M11, and M15), SEM imaging was performed. Fig. 14 displays the obtained SEM images of prepared samples. The SEM pictures demonstrated that the morphology of the new alkali activation phases was completely distinct from the raw materials. Since the WBP's alkaline-activation process with GGBS, aluminosilicate components were leached, creating a hydrated gel that was then cross-linked to form the stable, 3-dimensional network that can be seen in the microstructure photos (Fig. 14c and d). Whereas the WBP-based samples displayed a less dense structure with a higher number of unreacted aluminosilicate particles. This morphological variation may result from variations in the chemical makes-up, forms, and sizes of the WBP and GGBS [46-52]. Therefore, the AAC mixes should have a greater rate of alkali activation reaction after forming compressed and homogenous morphology than the WBP-based samples due to the presence of GGBS (Fig. 14a and c). On the other hand, WBP particles' high size caused incomplete alkali activation processes, which resulted in their less compact shape. Moreover, the generation of C-S-H/C(K)-A-S-H gels in the AAC mixtures was improved by the greater CaO content in GGBS. The microscopy photos demonstrate that the AAC samples become denser as the GGBS level rose. Between the 0% and 40% WBP combinations, there was a noticeable change. The M1 and M5 mixtures' loose and fractured appearance was seen in the SEM pictures. Moreover, the system contained a sizable number of embedded non-reacted or

partially reacted particles. The WBP system, which has a Si-O-Al-O structure, was exposed to more Ca2+ from GGBS as the fraction of GGBS in the system grew. From this point, it appeared that the M11 and M15 mixtures had a less dense and nonhomogeneous morphology with much less unreacted particles than the control mixture.

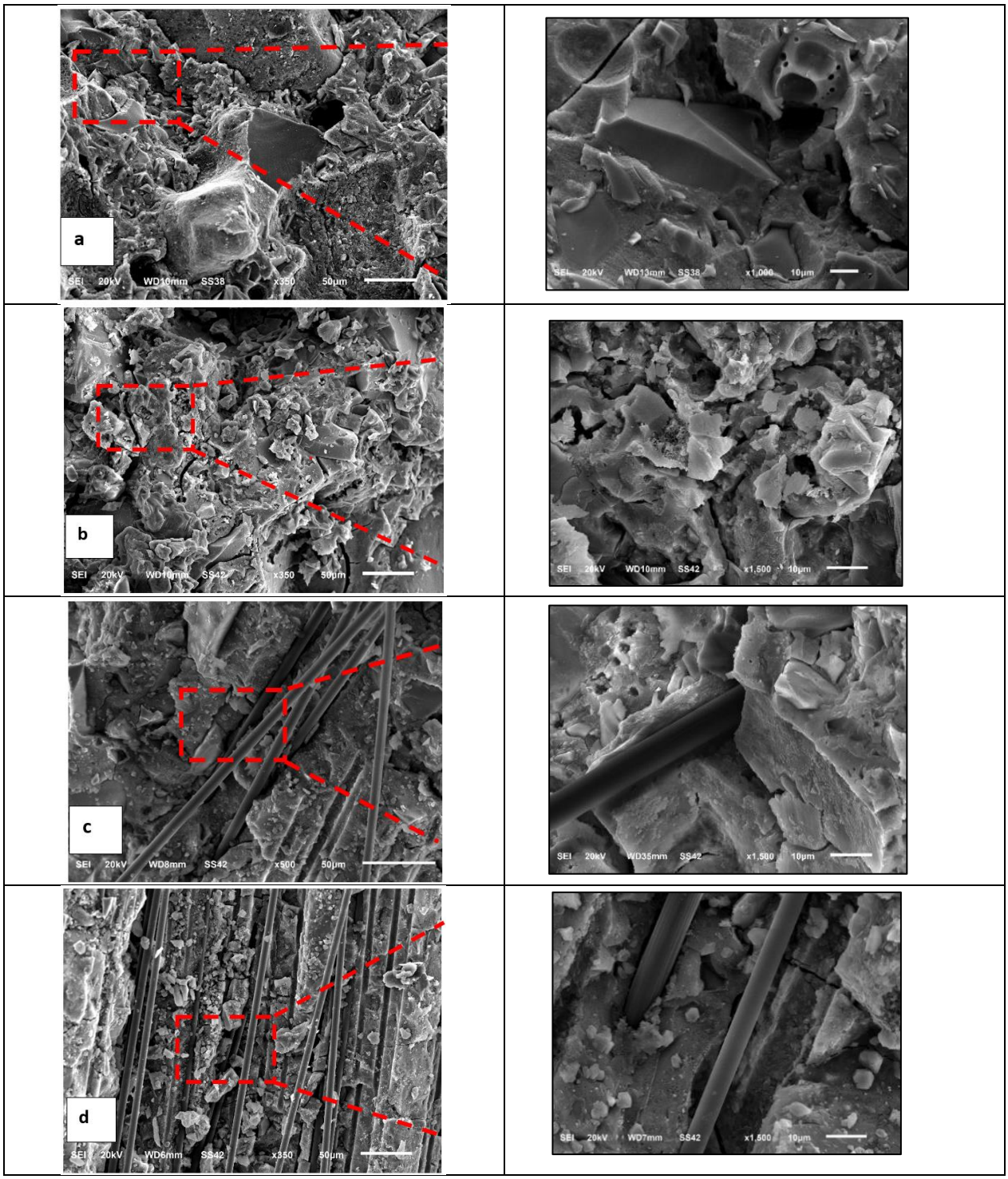

Fig. 14. Microstructure of the optimized AAC and WBP-based mixtures a) M1, b) M3, c)M5, d), M15.

Conclusions

In this study, the mix design of GGBS and WBP-based mixtures was enhanced using the Box-Behnken design, a statistical method for single-objective optimizes of 3 important variables. Also, the alterations in micro-structure, mineralogical phase, thermal decomposition, compressive strength, and flexural strength that occurring were examined. According to the experimental findings of this work, the following points o can be extracted:

Quadratic polynomial equations were used to represent the interaction between independent factors (WBP content, alkali activated concentration, and carbon fiber ratio) for early compressive strength. The optimum circumstances, as well as the general appeal of the predicted compressive strength values of 1 day (83.06 MPa) and 28 days (111.15 MPa), were 5% WBP content, a concentration of 1.90 alkali activators, and 1% carbon fiber content.

Highly workable AAC and WBP-based mixes were made using 40% WBP content. The WBP-based mixes' slump flow values ranged from 192 to 215 mm. It was also concluded that, with proper alkaline activation concentration and 40% WBP content, the compressive strength of AAC can exceed about 70 MPa.

The compressive strengths of the AAC in the presence of carbon fiber varied from 112-122 MPa after heat curing. The maximum strength value was achieved by the AAC with 0.5% carbon fiber and without addition of WBP (M5), while the lowest value was produced by the AAC with 0% carbon fiber (M1). While high WBP concentrations (above 40%) did not result in the development of high-strength AAC.

In contrast to WBP-based mixes, which showed a less dense microstructure and a higher proportion of unreacted aluminosilicate powders, AAC showed a well-dispersed, compact morphology.

Finally, the results of this study underscore even more how much promise there is in using recycled WBP to make high-strength AAC. WBP are therefore suitable replacement precursors that use less energy, enabling the production of environmentally friendly AAC.

References

[1] S. A. Miller, G. Habert, R. J. Myers, and J. T. Harvey, “Achieving net zero greenhouse gas emissions in the cement industry via value chain mitigation strategies,” One Earth, vol. 4, no. 10, pp. 1398–1411, 2021.

[2] M. Komljenovic et al., “Silico-Aluminophosphate and Alkali-Aluminosilicate Geopolymers: A Comparative Review,” vol. 6, p. 106, 2019, doi: 10.3389/fmats.2019.00106.

[3] P. Perez-Cortes and J. I. Escalante-Garcia, “Gel composition and molecular structure of alkali-activated metakaolin-limestone cements,” Cem Concr Res, vol. 137, Nov. 2020, doi: 10.1016/j.cemconres.2020.106211.

[4] A. M. Rashad, G. M. F. Essa, and H. A. Abdel-Gawwad, “An investigation of alkali-activated slag pastes containing recycled glass powder under the effect of elevated temperatures,” Environmental Science and Pollution Research, vol. 29, no. 19, pp. 28647–28660, Apr. 2022, doi: 10.1007/s11356-021-18365-7.

[5] J.-C. Lao, B.-T. Huang, Y. Fang, L.-Y. Xu, J.-G. Dai, and S. P. Shah, “Strain-hardening alkali-activated fly ash/slag composites with ultra-high compressive strength and ultra-high tensile ductility,” Cem Concr Res, vol. 165, p. 107075, 2023, doi: https://doi.org/10.1016/j.cemconres.2022.107075.

[6] S. Mabroum et al., “Formation of CSH and MSH gels in alkali-activated materials based on marl by-products from phosphate mines,” Constr Build Mater, vol. 365, p. 130029, 2023.

[7] S. Sasui et al., "Alkali activation of waste concrete powder: Effects of alkali type and concentration," Ceram Int, Feb. 2023, doi: 10.1016/J.CERAMINT.2023.01.224.

[8] I. N. A. Al-Duais, S. Ahmad, M. M. Al-Osta, M. Maslehuddin, T. A. Saleh, and S. U. Al-Dulaijan, "Optimization of alkali-activated binders using natural minerals and industrial waste materials as precursor materials," Journal of Building Engineering, vol. 69, p. 106230, Jun. 2023, doi: 10.1016/J.JOBE.2023.106230.

[9] R. Cai and H. Ye, "Clinkerless ultra-high strength concrete based on alkali-activated slag at high temperatures," Cem Concr Res, vol. 145, Jul. 2021, doi: 10.1016/j.cemconres.2021.106465.

[10] Abd Ellatief M, Abadel AA, Federowicz K, Abd Elrahman M. Mechanical properties, high temperature resistance and microstructure of eco-friendly ultra-high performance geopolymer concrete: Role of ceramic waste addition. Construction and Building Materials. 2023 Oct 19;401:132677.

[11] M. Abdellatief, S. M. AL-Tam, W. E. Elemam, H. Alanazi, G. M. Elgendy, and A. M. Tahwia, "Development of ultra-high-performance concrete with low environmental impact integrated with metakaolin and industrial wastes," Case Studies in Construction Materials, vol. 18, 2023, doi: 10.1016/j.cscm.2022.e01724.

[12] A. M. Tahwia, A. M. Heniegal, M. Abdellatief, B. A. Tayeh, and M. A. Elrahman, "Properties of ultra-high performance geopolymer concrete incorporating recycled waste glass," Case Studies in Construction Materials, p. e01393, Aug. 2022, doi: 10.1016/J.CSCM.2022.E01393.

[13] M. Nodehi and V. M. Taghvaee, "Alkali-Activated Materials and Geopolymer: a Review of Common Precursors and Activators Addressing Circular Economy," Circular Economy and Sustainability, vol. 2, no. 1, pp. 165–196, 2022, doi: 10.1007/s43615-021-00029-w.

[14] G. Görhan and G. Kürklü, "The influence of the NaOH solution on the properties of the fly ash-based geopolymer mortar cured at different temperatures," Compos B Eng, vol. 58, pp. 371–377, Mar. 2014, doi: 10.1016/J.COMPOSITESB.2013.10.082.

[15] Younis MO, Amin M, Tahwia AM. Durability and mechanical characteristics of sustainable self-curing concrete utilizing crushed ceramic and brick wastes. Case Studies in Construction Materials. 2022 Dec 1;17:e01251..

[16] Tahwia, A. M.; Elshikh, M. Y.; Elmetwaly, W.. Properties of Ultra High Strength Concrete Incorporating Nano-Silica. International Journal of Engineering Sciences & Research Technology, (2017), 6(5), 678-690. doi:10.5281/zenodo.800599.

[17] A. M. Tahwia, M. A. Ellatief, G. Bassioni, A. M. Heniegal, and M. A. Elrahman, "Influence of high temperature exposure on compressive strength and microstructure of ultra-high performance geopolymer concrete with waste glass and ceramic," Journal of Materials Research and Technology, vol. 23, pp. 5681–5697, Mar. 2023, doi: 10.1016/J.JMRT.2023.02.177.

[18] B. Luo and J. Dong, "Optimizing piezo resistivity of alkali-activated mortar using carboxylated multi-walled carbon nanotubes/basalt fibers," Mater Lett, vol. 329, p. 133151, Dec. 2022, doi: 10.1016/J.MATLET.2022.133151.

[19] H. Li et al., "Electrochemical oxidation of recycled carbon fibers for an improved interaction toward alkali-activated composites," J Clean Prod, vol. 368, p. 133093, Sep. 2022, doi: 10.1016/J.JCLEPRO.2022.133093.

[20] T. A. Hussein et al., "Chemical resistance of alkali-activated mortar with nano silica and polypropylene fiber," Constr Build Mater, vol. 363, p. 129847, Jan. 2023, doi: 10.1016/J.CONBUILDMAT.2022.129847.

[21] Abdellatief M, Elrahman MA, Alanazi H, Abadel AA, Tahwia A. A state-of-the-art review on geopolymer foam concrete with solid waste materials: components, characteristics, and microstructure. Innovative Infrastructure Solutions. 2023 Sep;8(9):230..

[22] S. Aydin and B. Baradan, "The effect of fiber properties on high performance alkali-activated slag/silica fume mortars," Compos B Eng, vol. 45, no. 1, pp. 63–69, Feb. 2013, doi: 10.1016/j.compositesb.2012.09.080.

[23] M. Tuyan, Ö. Andiç-Çakir, and K. Ramyar, "Effect of alkali activator concentration and curing condition on strength and microstructure of waste clay brick powder-based geopolymer," Compos B Eng, vol. 135, pp. 242–252, Feb. 2018, doi: 10.1016/J.COMPOSITESB.2017.10.013.

[24] B. Zhang, H. Zhu, Y. Cheng, G. F. Huseien, and K. W. Shah, "Shrinkage mechanisms and shrinkage-mitigating strategies of alkali-activated slag composites: A critical review," Constr Build Mater, vol. 318, p. 125993, Feb. 2022, doi: 10.1016/J.CONBUILDMAT.2021.125993.

[25] Tahwia, A. M.. Eco-Friendly Concrete Made with Recycled Aggregates. Life Sci J 2017; 14(4):121-128. 14(4), (2017). http://www.lifesciencesite.com. doi:10.7537/marslsj140417.16. 16.

[26] A. M. Tahwia, M. Abd Ellatief, A. M. Heneigel, and M. Abd Elrahman, "Characteristics of eco-friendly ultra-high-performance geopolymer concrete incorporating waste materials," Ceram Int, 2022, doi: 10.1016/j.ceramint.2022.03.103.

[27] R. Robayo-Salazar, W. Valencia-Saavedra, and R. Mejía de Gutiérrez, "Recycling of concrete, ceramic, and masonry waste via alkaline activation: Obtaining and characterization of hybrid cements," Journal of Building Engineering, vol. 46, p. 103698, Apr. 2022, doi: 10.1016/J.JOBE.2021.103698.

[28] A. A. Shahmansouri, M. Nematzadeh, and A. Behnood, "Mechanical properties of GGBFS-based geopolymer concrete incorporating natural zeolite and silica fume with an optimum design using response surface method," Journal of Building Engineering, vol. 36, p. 102138, Apr. 2021, doi: 10.1016/J.JOBE.2020.102138.

[29] W. Song et al., "Synthesis and characterization of eco-friendly alkali-activated industrial solid waste-based two-component backfilling grouts for shield tunnelling," J Clean Prod, vol. 266, p. 121974, Sep. 2020, doi: 10.1016/J.JCLEPRO.2020.121974.

[30] M. A. Villaquirán-Caicedo and R. Mejía de Gutiérrez, "Comparison of different activators for alkaline activation of construction and demolition wastes," Constr Build Mater, vol. 281, p. 122599, Apr. 2021, doi: 10.1016/J.CONBUILDMAT.2021.122599.

[31] Z. Li, D. Lu, and X. Gao, "Optimization of mixture proportions by statistical experimental design using response surface method - A review," Journal of Building Engineering, vol. 36, p. 102101, Apr. 2021, doi: 10.1016/J.JOBE.2020.102101.

[32] Z. Li, D. Lu, and X. Gao, "Multi-objective optimization of gap-graded cement paste blended with supplementary cementitious materials using response surface methodology," Constr Build Mater, vol. 248, p. 118552, Jul. 2020, doi: 10.1016/J.CONBUILDMAT.2020.118552.

[33] N. S. A. Yaro, M. Bin Napiah, M. H. Sutanto, A. Usman, and S. M. Saeed, "Modeling and optimization of mixing parameters using response surface methodology and characterization of palm oil clinker fine modified bitumen," Constr Build Mater, vol. 298, p. 123849, Sep. 2021, doi: 10.1016/J.CONBUILDMAT.2021.123849.

[34] B. S. Mohammed, V. C. Khed, and M. F. Nuruddin, "Rubbercrete mixture optimization using response surface methodology," J Clean Prod, vol. 171, pp. 1605–1621, Jan. 2018, doi: 10.1016/J.JCLEPRO.2017.10.102.

[35] R. Navarro, E. Zornoza, P. Garcés, I. Sánchez, and E. G. Alcocel, "Optimization of the alkali activation conditions of ground granulated SiMn slag," Constr Build Mater, vol. 150, pp. 781–791, Sep. 2017, doi: 10.1016/J.CONBUILDMAT.2017.06.064.

[36] Abdellatief M, Mortagi M, Abd Elrahman M, Tahwia AM, Alluqmani AE, Alanazi H. Characterization and optimization of fresh and hardened properties of ultra-high performance geopolymer concrete. Case Studies in Construction Materials. 2023 Dec 1;19:e02549.

[37] M. Abdellatief, W. E. Elemam, H. Alanazi, and A. M. Tahwia, "Production and optimization of sustainable cement brick incorporating clay brick wastes using response surface method," Ceram Int, 2022, doi: 10.1016/j.ceramint.2022.11.144.

[38] I. Ferdosian and A. Camões, "Eco-efficient ultra-high performance concrete development by means of response surface methodology," Cem Concr Compos, vol. 84, pp. 146–156, 2017, doi: https://doi.org/10.1016/j.cemconcomp.2017.08.019.

[39] M. Marzouki, B. Samet, and H. Tounsi, "Application of Plackett–Burman and Box-Behnken designs for the optimization of Tunisian dam sediment-based geopolymers," Journal of Building Engineering, vol. 50, p. 104162, Jun. 2022, doi: 10.1016/J.JOBE.2022.104162.

[40] E. Ghafari, H. Costa, and E. Júlio, "RSM-based model to predict the performance of self-compacting UHPC reinforced with hybrid steel micro-fibers," Constr Build Mater, vol. 66, pp. 375–383, 2014, doi: https://doi.org/10.1016/j.conbuildmat.2014.05.064.

[41] A. Aziz, A. Driouich, K. Felaous, and A. Bellil, "Box-Behnken design-based optimization and characterization of new eco-friendly building materials based on slag activated by diatomaceous earth," Constr Build Mater, vol. 375, p. 131027, Apr. 2023, doi: 10.1016/J.CONBUILDMAT.2023.131027.

[42] C. L. Hwang, M. Damtie Yehualaw, D. H. Vo, and T. P. Huynh, "Development of high-strength alkali-activated pastes containing high volumes of waste brick and ceramic powders," Constr Build Mater, vol. 218, pp. 519–529, Sep. 2019, doi: 10.1016/J.CONBUILDMAT.2019.05.143.

[43] C. L. Hwang, M. D. Yehualaw, D. H. Vo, T. P. Huynh, and A. Largo, "Performance evaluation of alkali activated mortar containing high volume of waste brick powder blended with ground granulated blast furnace slag cured at ambient temperature," Constr Build Mater, vol. 223, pp. 657–667, Oct. 2019, doi: 10.1016/J.CONBUILDMAT.2019.07.062.

[44] P. Rovnaník, B. Řezník, and P. Rovnaníková, "Blended Alkali-activated Fly Ash / Brick Powder Materials," Procedia Eng, vol. 151, pp. 108–113, Jan. 2016, doi: 10.1016/J.PROENG.2016.07.397.

[45] J. Fořt et al., "Application of waste brick powder in alkali activated aluminosilicates: Functional and environmental aspects," J Clean Prod, vol. 194, pp. 714–725, Sep. 2018, doi: 10.1016/J.JCLEPRO.2018.05.181.

[46] L. Deng et al., "Preparation and piezoresistive properties of carbon fiber-reinforced alkali-activated fly ash/slag mortar," Constr Build Mater, vol. 222, pp. 738–749, Oct. 2019, doi: 10.1016/J.CONBUILDMAT.2019.06.134.

[47] Amr B. ElDeeb, Vyacheslav N. Brichkin, Salah A. Salman, M. K. Gouda, Gamal S. Abdelhaffez, " Cost-effective and Eco-friendly extraction of alumina based on kaolin ore using thermo-chemically activated lime-sinter process", Journal of Al-Azhar University Engineering Sector, vol. 18, pp. 1 - 15, 2024.

[48] ElDeeb A.B., Brichkin V.N., Kurtenkov R.V., Bormotov I.S., 2021. Study of the peculiarities of the leaching process for self-crumbling limestone–kaolin cakes. Obogashchenie Rud, 2021, 27–32.

[49] I. Asadi, P. Shafigh, Z. F. Bin Abu Hassan, and N. B. Mahyuddin, "Thermal conductivity of concrete – A review," Journal of Building Engineering, vol. 20, pp. 81–93, Nov. 2018, doi: 10.1016/J.JOBE.2018.07.002.

[50] A. M. Tahwia, A. M. Heniegal, M. Abdellatief, B. A. Tayeh, and M. A. Elrahman, "Properties of ultra-high performance geopolymer concrete incorporating recycled waste glass," Case Studies in Construction Materials, vol. 17, 2022, doi: 10.1016/j.cscm.2022.e01393.

[51] El-Kholy AM, Tahwia AM, Elsayed MM. Prediction of simulated cost contingency for steel reinforcement in building projects: ANN versus regression-based models. International Journal of Construction Management. 2022 Jul 4;22(9):1675-89.

[52] Abd EL-Moatey AR, El-Rashed I, Al-Saed M, Soufy WH. Development of Geopolymer (Green) Cement Strength Without Natural And Chemicals Additive. Journal of Al-Azhar University Engineering Sector. 2019 Apr 1;14(51):469-84.